Carcinogenesis vol.31 no.8 pp.1465–1474, 2010
doi:10.1093/carcin/bgq109
Advance Access publication June 8, 2010

A bioluminescent mouse model of pancreatic β-cell carcinogenesis

Adrian Zumsteg, Karin Strittmatter, Daniela Klewe-Nebenius[1], Helena Antoniadis and Gerhard Christofori*

Department of Biomedicine, Institute of Biochemistry and Genetics and [1]Transgenic Mouse Core Facility, University of Basel, Basel, Switzerland

*To whom correspondence should be addressed. Department of Biomedicine, Institute of Biochemistry and Genetics, Center of Biomedicine, University of Basel, Mattenstrasse 28, 4058 Basel, Switzerland. Tel: +41 61 267 35 64; Fax: +41 61 267 35 66;
Email: Gerhard.christofori@unibas.ch

The Rip1Tag2 transgenic mouse model of pancreatic β-cell carcinogenesis has been instrumental in identifying several hallmarks of cancer, including tumor cell evasion from apoptosis, tumor angiogenesis and tumor invasion. Moreover, Rip1Tag2 mice have been helpful in the development and testing of innovative cancer therapies and tumor imaging protocols. However, based on tumor localization in the mouse, primary tumor growth and metastatic dissemination cannot be easily monitored in a longitudinal axis by non-invasive and low-technology approaches. Here, we report the generation of a new transgenic mouse line as a versatile tool to study β-cell carcinogenesis. Transgenic expression of a bicistronic messenger RNA encoding simian virus large T antigen and firefly luciferase in pancreatic β-cells recapitulates insulinoma development in a reproducible multistage process. In the mouse line called RipTag-IRES-Luciferase line (RTL) 1, the β-cell-specific expression of luciferase allows the non-invasive monitoring of primary tumor growth over time *in vivo* and the detection and quantification of disseminated tumor cells and micrometastases in distant organs *ex vivo*. When crossed to mouse lines in which the expression of cancer 'modifier' genes has been manipulated, tumor initiation and tumor progression are similarly affected as previously reported for Rip1Tag2 mice, indicating a robust tumor progression pathway shared between the two different transgenic mouse lines. Together, the data indicate that the RTL1 mouse line will be of great value to study anti-tumoral therapeutic approaches as well as to define the functional roles of cancer- and metastasis-related genes when crossed to appropriate transgenic or gene-targeted mouse lines.

Introduction

First transgenic mouse models of cancer have been established in the mid-1980s by the tissue-specific transgenic expression of oncogenes in mice resulting in the development of various cancer types (1). In the meantime, a plethora of murine cancer models has been established, and the range of transgenic tumor models has been expanded by models in which tumor suppressor genes have been inactivated by targeted recombination (knockout mice) or by chemical, pharmacological and hormonal induction protocols of cancer.

One of the first transgenic 'oncomouse' has been the Rip1Tag2 mouse line, expressing SV40 large T antigen (Tag) under the control of the rat insulin promoter (Rip) and recapitulating tumorigenesis of the pancreatic β-cells in the islets of Langerhans (2). This mouse model has been widely used as a model of multistage tumorigenesis in cancer research and, together with others, has substantially contributed to the concept summarized as 'hallmarks of cancer' (3). Notably, the Rip1Tag2 transgenic mouse model has been instrumental in visualizing the onset of tumor angiogenesis (the 'angiogenic switch'), a highly regulated process that is mainly governed by the expression of pro-angiogenic growth factors, including vascular endothelial growth factor A (VEGF)-A (4–6). The gain of survival signaling to overcome apoptosis during tumor development has been demonstrated by the upregulated expression of insulin-like growth factor II (IGF-II) during Rip1Tag2 tumorigenesis (7). Finally, Rip1Tag2 mice have been instrumental to demonstrate the critical role of cell adhesion molecules, such as E-cadherin, during malignant tumor progression and metastasis (8). Another critical feature of cancer development is the interaction of a tumor with its microenvironment and inflammatory cells that promote tumor growth, angiogenesis and invasion and help the tumor to evade immune surveillance (reviewed in ref. 9). Also here, Rip1Tag2 mice have been employed to define the critical role of bone marrow-derived cells, such as neutrophils, in supplying matrix metalloproteinase 9, which can activate matrix-sequestered VEGF-A and thus tumor angiogenesis (6,10). Finally, Rip1Tag2 mice have been employed to develop novel radiopeptide-mediated imaging of insulinoma, currently being tested in the clinics (11).

Despite its established usefulness for basic and translational cancer research, the Rip1Tag2 model has also its limitations. Islets of Langerhans and the tumors derived thereof are buried deep in the mouse body, rendering it difficult to monitor tumor growth in living mice in longitudinal analyses. Even though many preclinical studies have been undertaken with Rip1Tag2 mice (12–18), the necessity to set a defined end point due to unknown tumor growth diminishes the flexibility in the analysis of this cancer model. Another drawback of the Rip1Tag2 mouse model is its transgene integration site. The close proximity to the glucagon gene causes aberrant expression of T antigen in gastrointestinal L cells, occasionally giving rise to intestinal neuroendocrine carcinoids and hampering the analysis of β-cell tumorigenesis (19,20).

Here, we report the generation and characterization of an improved version of the Rip1Tag2 mouse model in which firefly luciferase is expressed in addition to SV40 T antigen specifically in the pancreatic β-cells [RipTag-IRES-Luciferase (RTL) 1]. In these mice, tumor growth can be monitored non-invasively by bioluminescence analysis, and metastatic events can be easily monitored by luciferase activity in distant organs *in vivo* and *ex vivo*. Moreover, in RTL1 mice, expression of T antigen is highly restricted to pancreatic β-cells, and no other tumor type occurs. Finally, the reproducible recapitulation of all distinct tumor stages observed in human cancer, including the onset of angiogenesis and occasional lymph node and distant metastasis, make it a suitable model for genetic and pharmacological experimentation.

Materials and methods

Generation of RipTag-IRES-Luciferase transgenic mice

A DNA fragment containing the rat insulin promoter 1 regulatory region, the SV40 early region, followed by an internal ribosomal entry site (IRES), the firefly luciferase coding region and the SV40 early polyadenylation signal was generated as described in supplementary Methods (available at *Carcinogenesis* Online). The linearized transgene construct was microinjected into pronuclei of fertilized FVB/N eggs according to standard techniques (21). Genomic polymerase chain reaction (PCR) identified three founder lines designated RTL1, 2 and 3. All other transgenic mouse lines have been previously reported (22–26). All experiments involving mice were performed in accordance with the guidelines of the Swiss Federal Veterinary Office and the regulations of the Cantonal Veterinary Office of Basel-Stadt.

In vivo bioluminescence

Prior to measurement, mice were shaved in the peritoneal region and injected *intraperitoneally* with D-luciferin potassium salt (Gold BioTechnology, St Louis, MO) dissolved in sterile phosphate-buffered serum at 15 mg/ml with

Abbreviations: BrdU, bromodeoxyuridine; IGF-II, insulin-like growth factor II; IGF1R, insulin-like growth factor receptor 1; LYVE-1, lymphatic vessel endothelial hyaluronan receptor 1; MDSC, myeloid-derived suppressor cells; mRNA, messenger RNA; NCAM, neural cell adhesion molecule; PCR, polymerase chain reaction; RTL, RipTag-IRES-Luciferase; SEM, standard error of the mean; VEGF, vascular endothelial growth factor A.

a luciferin dose of 150 mg/kg body weight. Five minutes after luciferin injection, mice were anaesthetized by inhalation of 3% isoflurane (Provet AG, Lyssach, Switzerland) and placed in the dark chamber of the 'NightOWL II LB 983' imaging system (Berthold Technologies, Bad Wildbad, Germany). For quantification experiments with multiple rounds of monitoring, timing of injection, anesthesia and camera setting were standardized and kept constant throughout the experiment. Typical acquisition times were between 1 and 5 min with maximal binning. For quantification of light intensities in time course experiments, a constant analysis gate was defined and individual tumor photon counts were determined by centering the gate on the highest signal intensity for each time point.

Fluorescence-activated cell sorting analysis

Peripheral blood was drawn directly by heart puncture of CO_2 killed mice and transferred to ethylenediaminetetraacetic acid anti-coagulated collection tubes (Sarstedt, Sevelen, Switzerland). For details of the fluorescence-activated cell sorting analysis, see supplementary Methods (available at *Carcinogenesis* Online).

Quantitative real-time reverse transcription–PCR

Total RNA from tumors or total pancreas was prepared using TRI Reagent (Sigma, Buchs, Switzerland) and reverse transcribed with random hexamer primers using moloney murine leukemia virus reverse transcriptase (Sigma). Complementary DNA was quantified on an ABI Prism 7000 light cycler (Applied Biosystems, Zug, Switzerland) using SYBR green PCR MasterMix (Fermentas) using the primers described in supplementary Table S2 (available at *Carcinogenesis* Online). C_t values were normalized against ribosomal protein L19 (RPL19) and fold induction was calculated as $2\Delta\Delta^{C_t}$

Quantification of luciferase activity

Organs and tumors were homogenized into precooled Reporter Lysis Buffer (Promega, Duebendorf, Switzerland). Samples were cleared by cetrifugation and supernatants stored at −20°C until further analysis. For quantification, 10 µl of lysate was mixed with 50 µl of Luciferase Assay Reagent (Promega) and luminescence measured on a Centro LB 960 luminometer (Berthold Technologies). Liver and lung lysates were found to have a high quenching activity and were used in a 1:5 dilution.

Histology and immunostaining

See supplementary Methods available at *Carcinogenesis* Online.

Statistical evaluation

All statistical tests were performed using GraphPad Prism 4.0c for Mac. Data were first tested for normality and when normality was fulfilled, unpaired two-tailed Student's *t*-test was applied. For non-Gaussian data, Mann–Whitney non-parametric *U*-test was performed. Survival data were analyzed by log-rank test. P values <0.05 were considered statistically significant.

Results

Generation of transgenic RTL mice

An expression cassette was generated in which SV40 large T antigen and firefly luciferase are expressed in a bicistronic manner under the control of the rat insulin promoter specifically in β-cells of the islets of Langerhans (supplementary Figure S1A is available at *Carcinogenesis* Online). The linearized plasmid construct was then used to generate transgenic mice in the FVB/N genetic background. Three founder lines, termed RTL1, 2 and 3, developed fatal insulinomas. In lines RTL2 and 3, only males developed tumors (within 25 weeks), even though the transgene had not integrated in the Y chromosome. The levels of messenger RNA (mRNA) encoding for large T antigen in islets of Langerhans from young non-tumor-bearing mice were found 12- to 20-fold lower in RTL2 and 3 mice as compared with RTL1 mice (data not shown).

In vivo bioluminescence signals were aberrant in lines RTL2 and 3, whereas in the RTL1 line, tumors as small as 2 mm could be detected at the expected site located in the higher peritoneal region (Figure 1A). Tissue-specific expression of the transgene was determined by analyzing luciferase activity in organ lysates from 6- to 8-week-old RTL mice, when the mice were still tumor free. Luciferase activity levels were very low in most of the organs analyzed (supplementary Figure S1B is available at *Carcinogenesis* online). Testis and fat tissue lysates were positive in all mouse lines, indicating baseline activity of the rat insulin promoter in this organ. Preputial gland was positive in lines RTL2 and 3, and males of the line RTL3 showed aberrant luciferase expression in the skin. However, besides tumors of pancreatic β-cells, no other tumor type was detected in the three transgenic lines. Based on its robust and reproducible transgene expression and tumor development, line RTL1 was selected for further experimentation.

We next determined the transgene integration site in the RTL1 line by linker-mediated PCR. The single integration site was localized distal to the H4 region of chromosome 3, 100 and 500 kb apart from the next annotated genes (supplementary Figure S1C is available at *Carcinogenesis* Online). Quantitative PCR on genomic DNA revealed that RTL1 mice carried ∼40 transgene copies per heterozygous genome as compared with five copies in Rip1Tag2 mice (data not shown). Mice homozygous for the RTL1 transgene did not show any abnormalities, indicating negligible distortion of the genomic locus (supplementary Figure S1D is available at *Carcinogenesis* Online). Nevertheless, all the experiments reported here have been performed with heterozygous RTL1 mice.

Lysates from RTL1 tumors exhibited very high luciferase expression levels (supplementary Figure S2A is available at *Carcinogenesis* Online), about three to five orders of magnitude above the levels detected in liver and lung, two potential target organs of insulinoma metastasis. The variability in luciferase activities found between individual tumors might reflect the different levels of insulin expression in insulinomas (Figure 4C) as well as varying relative proportions of tumor cells constituting the tumor mass. Two cell lines derived from tumors of RTL1 mice showed significantly higher levels of luciferase activity than primary tumors (supplementary Figure 2A is available at *Carcinogenesis* Online). One of these cell lines homogeneously expressed T antigen and insulin (Figure 1B) and denoted the upper limit of luciferase expression in the RTL1 system.

Tumors of RTL1 mice expressed about four times more T antigen transcript as compared with tumors of Rip1Tag2 mice, a finding confirmed by immunoblotting analysis (Figure 1C, data not shown). In contrast, T antigen mRNA levels were ∼2-fold higher in total pancreata from newborn Rip1Tag2 mice as compared with newborn RTL1 mice.

Kinetics of tumor development

In our laboratory, Rip1Tag2 mice are usually bred in the C57Bl/6 background, and the average life span of these mice is ∼12.6 weeks. Average tumor volumes of Rip1Tag2 mice at 12 weeks are ∼36 mm^3. In contrast, RTL1 mice in FVB/N background have a median survival of 20.7 weeks, with a median survival of 19.4 weeks for female and 22.0 weeks for male mice (supplementary Figure S2B is available at *Carcinogenesis* Online). At age 18–20 weeks, tumor volumes of RTL1 female versus male mice did not significantly differ, with an average tumor volume of 99 ± 29 mm^3 and 65 ± 12 mm^3 for females and males, respectively [Figure 1D, mean ± standard error of the mean (SEM)]. However, at age 21–22 weeks, average tumor size of females was lower (37 ± 11 mm^3) as compared with males (233 ± 33 mm^3) (Figure 1D). At this age, males have a significantly higher survival rate than females, indicating that females alive at this age have a delayed tumor progression, whereas males can live under higher tumor burden. The kinetics of tumor development in RTL1 mice appeared to be unchanged in a pure FVB/N background versus C57/FVB mixed background (supplementary Figure S2B is available at *Carcinogenesis* Online), indicating a certain independence of RTL1 tumorigenesis from the genetic background.

To assess how RTL1 tumor development is affected by the activity of factors known to modify tumor progression, RTL1 mice were crossed to mice expressing tumor 'modifier' genes in pancreatic β-cells under the control of the rat insulin promoter. These mouse lines have been previously characterized, also by intercrossing them with the Rip1Tag2 tumor model. For example, transgenic expression of VEGF-A accelerates tumor growth in Rip1Tag2 mice without affecting metastases (22), whereas VEGF-C and VEGF-D promote tumor lymphangiogenesis and lymph node metastases (23,25). Insulin-like growth factor receptor 1 (IGF1R) over-expression

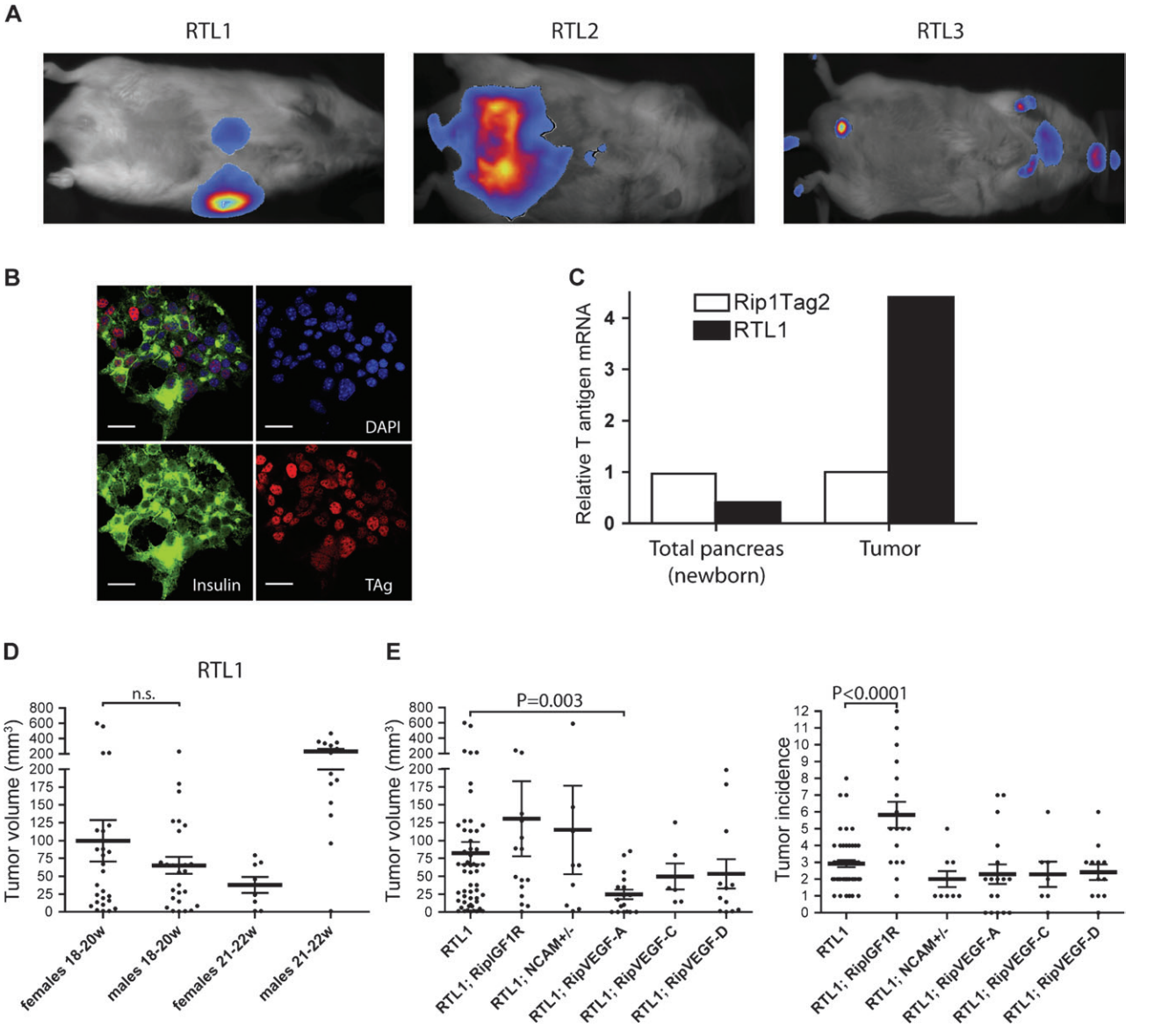

Fig. 1. *In vivo* bioluminescence and tumor detection. (**A**) *In vivo* luciferase bioluminescence analysis of transgenic mouse lines RTL1, 2 and 3. (**B**) Cell lines derived from RTL1 tumors show homogeneous insulin and SV40 large T antigen expression as determined by immunofluorescent staining; scale bar: 20 μm. (**C**) T antigen mRNA expression in total pancreas and tumors of newborn and adult Rip1Tag2 and RTL1 mice, respectively, as determined by quantitative reverse transcription–PCR. (**D**) RTL1 males and females exhibit similar tumor volumes before 20 weeks of age, whereas at the age of 22 weeks, male mice develop larger tumors. (**E**) Tumor volumes in single-transgenic RTL1 and in composite double-transgenic RTL1;RipIGF1R, RTL1;RipVEGF-C, RTL1;RipVEGF-D and RTL1;NCAM$^{+/-}$ mice. Shown are individual values with means ± SEMs. For statistical test see supplementary Table S1 (available at *Carcinogenesis* Online).

promotes tumor growth and progression in Rip1Tag2 mice (24), and neural cell adhesion molecule (NCAM) deficiency causes lymph node metastases by decreasing tumor–extracellular matrix adhesion and increasing tumor lymphangiogenesis (26,27).

As previously reported for Rip1Tag2 mice, composite transgenic mice of RTL1;RipVEGF-C, RTL1;RipVEGF-D and RTL1;NCAM$^{+/-}$ genotype, no difference in survival was observed. In contrast, as also reported before for Rip1Tag2 mice, transgenic co-expression of VEGF-A or IGF1R under the Rip promoter caused a drastic highly significant survival reduction in RTL1;RipVEGF-A and RTL1;RipIGF1R mice (supplementary Figure 2C and D is available at *Carcinogenesis* Online).

No significant changes in tumor volume or incidence were seen in RTL1 mice crossed to RipVEGF-C, RipVEGF-D or NCAM$^{+/-}$ composite mice (Figure 1E, supplementary Table S1, available at *Carcinogenesis* Online), a result comparable with previously published data on RipVEGF-C, RipVEGF-D and NCAM$^{+/-}$ in Rip1Tag2 mice. In contrast, RTL1;RipIGF1R had larger and twice as many macroscopic tumors than RTL1 mice (Figure 1E, supplementary Table S1, available at *Carcinogenesis* Online), even though they were analyzed at only 9–11 weeks of age (versus 18–20 weeks in single-transgenic RTL1 mice), highlighting the role of IGF1R as a tumor progression factor. Curiously, RTL1;RipVEGF-A double-transgenic mice had significantly smaller tumors than RTL1 mice at time of death (Figure 1E, supplementary Table S1, available at *Carcinogenesis* Online). Tumor lysates derived from these composite mice did not exhibit significantly different luciferase activities, indicating that the expression of modifier genes had no significant impact on transgene expression (supplementary Figure S2A, available at *Carcinogenesis* Online).

Bioluminescence quantification of tumor growth in vivo

As described above, luciferase activities varied largely between different tumors of RTL1 mice. Bearing this in mind, tumor growth was monitored in individual mice over a period of 4 weeks by *in vivo*

bioluminescence once or twice weekly. Signal intensity was maximal ~10 min after D-luciferin injection and stayed at plateau levels for 20–30 min (data not shown). As tumors were localized at various sites and depths within the pancreas, absolute luciferase intensities and thus tumor sizes could not be directly compared between different mice. Yet, for individual mice, an increase in luciferase activity and thus tumor growth could be monitored over time (Figure 2A). Analysis of a large cohort of mice revealed a 3-fold increase in normalized signal intensity over the analysis period of 4 weeks (Figure 2B).

Tumor progression

Hyperplastic islets and dysplastic angiogenic islets were detected in RTL1 mice as early as 7 weeks of age, as visualized by bromodeoxyuridine (BrdU) incorporation in hyperplastic but not in normal islets and by increasing vessel densities and hemorrhages in angiogenic islets. Beginning at 10 weeks of age, macroscopic tumors could be detected. The low abundance of macroscopic tumors in RTL1 mice detected by bioluminescence was confirmed by histopathological analysis. According to the previously reported classification of Rip1-Tag2 tumors (8), we classified the stages of tumor development in RTL1 mice into the following categories: normal islets, hyperplastic islets, angiogenic islets, adenoma and carcinomas of grade 1 (micro-invasive), grade 2 (fully invasive) and grade 3 (anaplastic) (Figure 3A; data not shown). In grade 2 tumors, detached tumor cell clusters were often detected within the tumor (Figure 3B) and in blood vessels within the exocrine pancreas (Figure 3C), indicating tumor disaggregation and tumor cell dissemination. In general, pancreata of Rip1-Tag2 mice showed a higher abundance of tumors as compared with RTL1 mice (Figure 3D). Per pancreatic tissue section from RTL1 mice was analyzed at the age of 18–20 weeks, in average 5.5 ± 1.8 normal/hyperplasic islets, 5.5 ± 1.6 adenoma and 1.6 ± 0.3 carcinoma were detectable (mean per mouse ± SEM, 6 mice, 76 counted lesions). BrdU injection 2 h before killing and staining for incorporated BrdU revealed a proliferation rate of 10.1 ± 0.7% of all tumor-constituting cells (mean of microscopic fields ± SEM; 3 mice, 12 tumors, 27 microscopic fields). TdT-mediated dUTP-biotin nick end labeling staining revealed 1.05 ± 0.08% apoptotic cells within tumors (mean of microscopic fields ± SEM; 4 mice, 9 tumors, 25 microscopic fields). Tumor hypoxia was analyzed by immunohistochemical staining for the hypoxia-inducible factor 1 alpha target gene carbonic anhydrase IX (Ca-IX; reviewed in ref. 28). Ca-IX staining was found absent or very low in tumors of both Rip1Tag2 and RTL1 mice (supplementary Figure S3A, available at *Carcinogenesis* Online), indicating low tumor hypoxia in both mouse models. Interestingly, in Rip1Tag2 but not in RTL1 mice, the tumor-surrounding exocrine tissue upregulated Ca-IX expression in the vicinity of the invasion fronts of carcinoma.

Immunohistochemical staining of tumor sections with antibodies against CD31 revealed that larger tumors were less vascularized toward the tumor center as compared with the outer rims (Figure 4A). NG2, a proteoglycan indicative for pericytes, strictly colocalized with blood vessels in the tumor periphery (Figure 4A). In contrast, although widely devoid of CD31-positive vessels, central tumor regions contained NG2-positive pericytes, possibly as remnants of previously intact tumor vasculature.

We next assessed the expression of E-cadherin, an epithelial marker expressed in β-cells of Langerhans islets and reduced in its expression during the transition from adenoma to carcinoma during Rip1Tag2 tumorigenesis (26). In RTL1 mice, E-cadherin expression was found to be retained in hyperplastic islets and adenoma but was lost in the invasive areas of grade 1 carcinoma and in all of grades 2 and

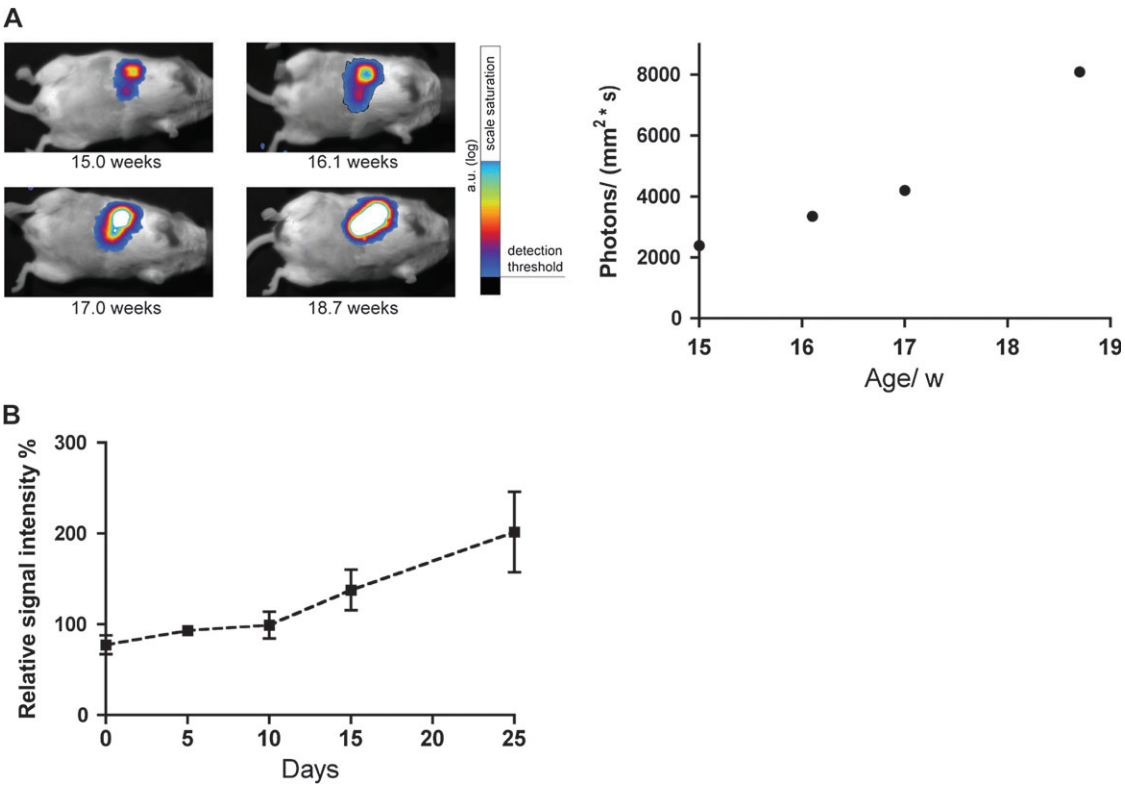

Fig. 2. *In vivo* bioluminescence of tumor growth over time. (**A**) Longitudinal analysis of luciferase bioluminescence in an individual RTL1 mouse over 4 weeks shows increasing light emission over time. The same scale was used for all four images causing signal intensities out of scale at age 17 and 18.7 weeks (white central area inside false colored area). Right panel: photon flow quantification of the (false) colored area in left panel. (**B**) Tumor growth in a cohort of 12 mice (average age at first monitoring: 15 weeks) was followed over 25 days by *in vivo* bioluminescence. The signal intensities were normalized for each mouse individually, with 100% representing the geometrical mean of all values obtained per mouse during the 25 days observation period. Shown are means of the 12 mice ± SEMs.

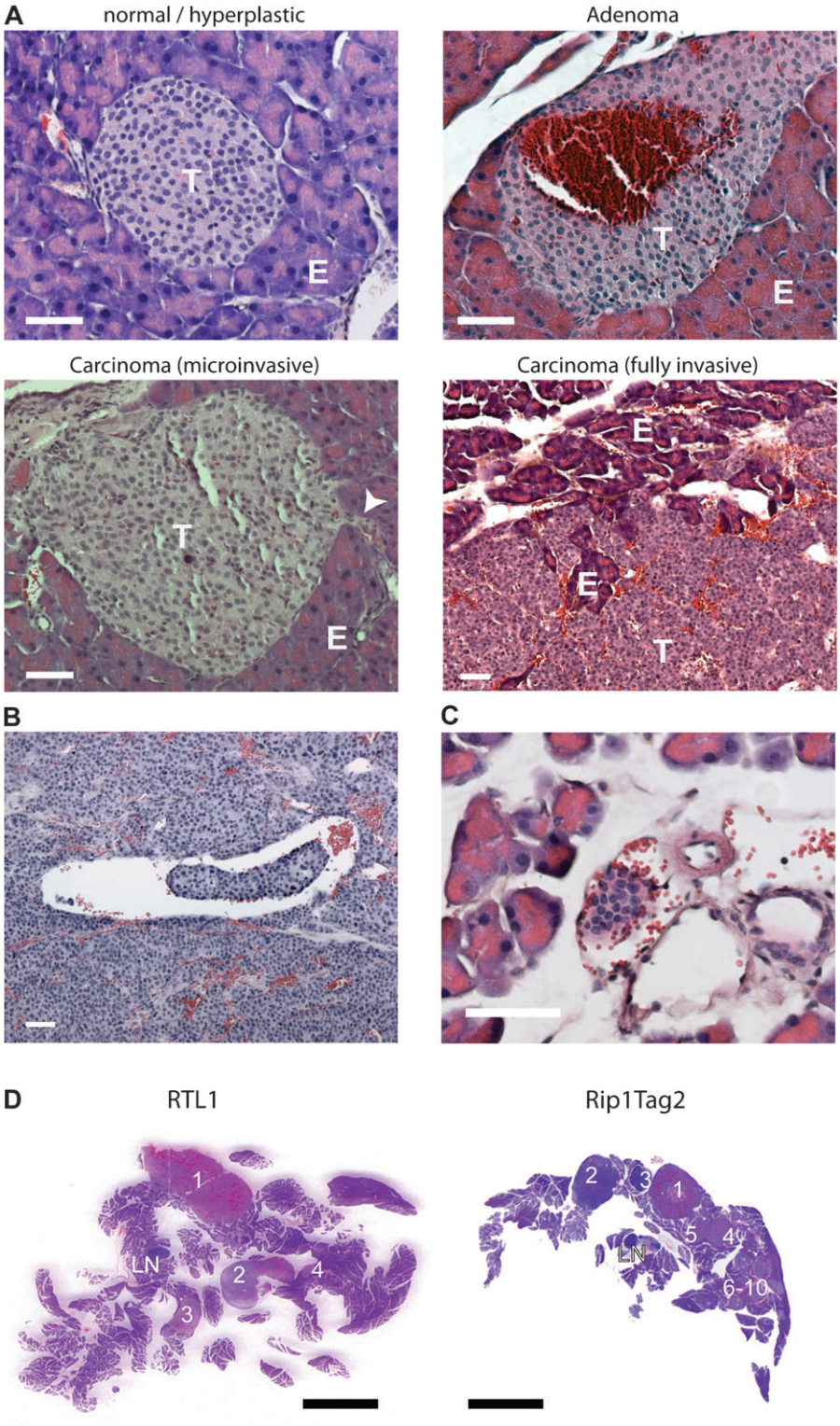

Fig. 3. Tumor progression in RTL1 mice. (**A**) Representative hematoxylin and eosin staining of histological sections from the various stages of tumor development in RTL1 mice. (**B**) Disaggregated tumor cell clusters are found in hemorrhagic areas of RTL1 tumors. (**C**) In RTL1 mice, tumor cell clusters are found in blood vessels within the exocrine pancreas as identified by the presence of erythrocytes and a clearly defined vascular lining. (**D**) Histological sections of total pancreata of RTL1 and Rip1Tag2 mice stained with hematoxylin and eosin indicate that RTL1 mice have fewer lesions. Numbers indicate tumors >1 mm in diameter within the sections. T: tumor, E: exocrine pancreas, LN: lymph node. Scale bars: (A–C): 50 μm and (D): 5 mm.

3 carcinoma (Figure 4B). Similar observations were made for insulin, a characteristic β-cell marker. Lesions up to grade 1 retained insulin expression, albeit at reduced levels compared with normal islets, whereas grade 2 carcinoma eventually downregulated insulin expression in certain areas (Figure 4C). In order to determine major transcriptional changes that could be involved in the differential regulation of tumor onset and progression between RTL1 and Rip1-Tag2 mice, we analyzed the expression of genes known to be critical

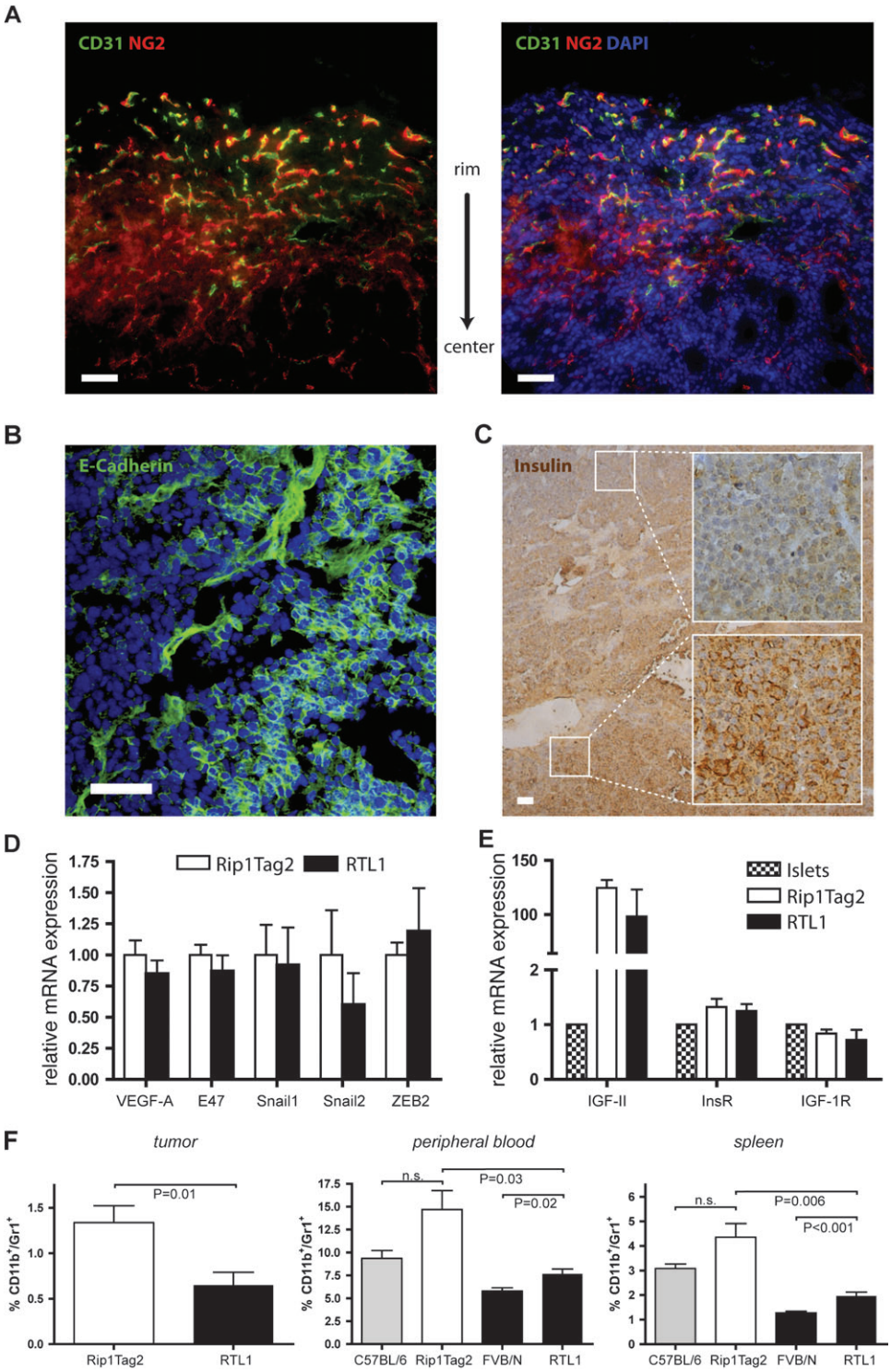

Fig. 4. Analysis of tumor angiogenesis and tumor progression in RTL1 transgenic mice. (**A**) Immunofluorescent staining of RTL1 tumors with antibodies against the endothelial marker CD31 (green) and the pericyte marker NG2 (red). The background observed in the red fluorescent channel originates from blood hemorrhages. 4′,6-Diamidino-2-phenylindole (DAPI) visualizes nuclei (blue). (**B**) Fluorescent staining for E-cadherin (green) in an area of a grade 2 carcinoma where E-cadherin has been lost in the invasive β tumor cells yet is maintained in non-invasive cells. DAPI visualizes nuclei (blue). (**C**) Immunohistochemical staining of an RTL1 carcinoma with antibodies against insulin (brown). A partial downregulation of insulin expression is apparent in the dedifferentiated regions of the tumor. (**D** and **E**) Gene expression analysis in macroscopic tumors of Rip1Tag2 and RTL1 mice by quantitative real-time PCR. (D) No significantly different mRNA levels of the angiogenic factor VEGF-A or the transcriptional repressors E47, Snail1, Snail2 or ZEB2 were detected ($N = 3$–8 individual tumors from each genotype). (E) Insulinomas upregulate IGF-II compared with islets but the receptor levels are unchanged (two individual islet isolations, $N = 8$ individual tumors for Rip1Tag2 and $N = 4$ for RTL1). (**F**) Fluorescence-activated cell sorting analysis of immune cell infiltration into tumors of RTL1 or Rip1Tag2 mice. *P*-values from unpaired two-tailed Student's *t*-test. Shown are means ± SEMs. Scale bars: 50 μm.

for tumor progression by quantitative PCR, including VEGF-A and the major transcriptional repressors of E-cadherin gene expression, Snail1, Snail2, Zeb1 and Zeb2 (Figure 4D). However, none of these factors was differentially expressed between tumors of Rip1Tag2 and RTL1 mice.

Previously, we have shown that IGF-II provides critical survival signals for Rip1Tag2 tumorigenesis. Its expression correlates with hyperproliferation, and growth of Rip1Tag2 tumors is severely impaired in IGF-II knockout mice (7). Similar to tumors in Rip1Tag2 mice, tumors in RTL1 mice showed very high expression of IGF-II as compared with islets of Langerhans (Figure 4E). In contrast, expression of insulin receptor (InsR) and IGF1R, known receptors for IGF-II, was unchanged between islets, Rip1Tag2 and RTL1 tumors (Figure 4E). Together, these data indicate that tumor progression in RTL1 mice is highly comparable with the multistage tumorigenesis observed in Rip1Tag2 mice in various histopathological and molecular parameters.

Reduced infiltration by myeloid-derived suppressor cells

However, there are also significant differences between tumor development in RTL1 and Rip1Tag2 mice. In addition to tumor cell-intrinsic factors, it is now well established that myeloid cells can be critical components in promoting tumor angiogenesis and metastasis as well as in protection from adaptive immune responses (reviewed in ref. 9). In particular, myeloid-derived suppressor cells (MDSC), characterized by a concomitant expression of the myeloid marker CD11b and the granulocyte marker Gr1, have been demonstrated to suppress activation of dendritic and cytotoxic T cells, and their abundance usually increases in peripheral blood and spleen with increasing tumor size. By flow cytometry, we detected an increase in $CD11b^+/Gr1^+$ MDSC levels in peripheral blood and spleen of insulinoma-bearing mice as compared with their non-tumor-bearing inbred strain. Notably, FVB/N mice have significantly less MDSC in peripheral blood and spleen as compared with C57BL/6 mice, and consistent with this notion, we found significantly less MDSC infiltrating the tumors of RTL1 mice as compared with tumors from Rip1Tag2 mice (Figure 4F, left panel), a difference that was also detected in spleen and peripheral blood of tumor-bearing mice (Figure 4F, middle and right panels).

In order to assess early events that might explain the delayed tumor progression in RTL1 mice as compared with Rip1Tag2 mice, we analyzed the presence of tumor infiltrating lymphocytes in 8-week-old mice. Whereas no B lymphocyte infiltration was evident (data not shown), T lymphocytes were present at comparable levels in lesions of both strains (supplementary Figure S3B and C is available at *Carcinogenesis* Online). In contrast, levels of infiltrating $F4/80^+$ macrophages were significantly reduced in RTL1 mice as compared with Rip1Tag2 mice (supplementary Figure S3B and C is available at *Carcinogenesis* Online). Signs of T lymphocytes attacking hyperplastic islets, such as massive islet cell death or aggregates of T lymphocytes, were not apparent. In contrast, hyperplastic islets of RTL1 mice showed a 3-fold decrease of the proliferation marker phospho-Histone H3 as compared with Rip1Tag2 mice (supplementary Figure S3B and C is available at *Carcinogenesis* Online), which could result from the lower levels of T antigen expression in RTL1 mice (Figure 1C).

Lymph node and liver metastasis

Next, we assessed the metastatic dissemination of tumor cells and the formation of metastasis in RTL1 mice. Histological analysis of pancreatic lymph nodes revealed lymph node metastases in 3 of 13 mice with a total of 23 lymph nodes analyzed (Figure 5A). Since insulinoma is known to metastasize to liver and lung both in man (29) and in mice (30), the presence of tumor cells in these organs was analyzed in RTL1 single-transgenic mice by *in vitro* luciferase assays between 18 and 20 weeks of age. Luciferase activity was found increased at least 3-fold above background in the livers of 19 of 66 mice (29%). Primary tumor size significantly correlated with luciferase activity in liver lysates (Figure 5B), and mice carrying primary tumors above a tumor volume of 150 mm^3 exhibited a 67% likelihood of liver metastasis (Table I). The occurrence of liver metastasis was confirmed by the presence of insulin-positive nodules in the liver (Figure 5C). Up to 20 of these insulin-positive structures were detectable in one histological section of the livers of RTL1 mice, yet they never reached macroscopic size and remained below a diameter of 150 μm. Liver metastases showed no hypoxia as analyzed by Ca-IX staining (data not shown) and were also detected in RTL1;RipIGF1R, RTL1;$NCAM^{+/-}$ and RTL1;RipVEGF-C composite mice by *in vitro* luciferase assays of organ lysates (Figure 5D and Table I) and by insulin staining of liver sections (data not shown). RTL1;RipIGF1R double-transgenic mice developed more metastasis than single-transgenic RTL1 mice.

The hepatic metastatic clusters in RTL1 mice were partially or completely surrounded by CD31- and lymphatic vessel endothelial hyaluronan receptor 1 (LYVE-1)-positive vessels (Figure 5E). In contrast to many other organs in which LYVE-1 is a marker for lymphatic vessels (31) or a subset of macrophages (32), hepatic sinusoidal endothelial cells also express LYVE-1 (33). The blood endothelial character of the vessels surrounding the metastatic nodules was further highlighted by the erythrocytes present in the vessels (Figure 5C). Most metastatic nodules were negative for the epithelial marker E-cadherin, which is absent in most grade 2 primary carcinomas (Figure 5E). Yet, within larger metastatic clusters, we found small patches of cells expressing E-cadherin, indicating re-differentiation of metastatic cells. Immunohistochemical staining for phospho-Histone-3 revealed proliferating cells within the metastatic nodules (Figure 5E).

Analysis of luciferase activities in lysates of various organs from RTL1 mice revealed high levels in the lungs of 3 of 45 RTL1 mice, in 1 of 14 RTL1;RipVEGF-D mice and in 2 of 4 RTL1;RipIGF1R mice, whereas in RTL1;RipVEGF-C, RTL1;RipVEGF-A and RTL1;$NCAM^{+/-}$ mice we did not detect any increased activities in lung. In contrast to liver, we were not able to detect metastases by histology in the contralateral lung lobe to the one used for *ex vivo* luciferase analysis. In brain, we detected luciferase values above background levels in only a few mice, and histological analysis of brain sections also did not reveal any apparent micrometastasis.

Discussion

The Rip1Tag2 tumor model has proven to be extremely instructive in identifying cellular processes and molecular pathways participating in multistage tumorigenesis, including the molecular mechanisms underlying the so-called angiogenic switch, tumor cell survival and tumor invasion. Moreover, based on the high reproducibility of the multiple stage of tumorigenesis in Rip1Tag2 transgenic mice, they have also been frequently employed for preclinical testing of experimental drugs. Yet, due to the location of insulinoma within the pancreas, Rip1Tag2 mice cannot be easily employed to monitor tumor growth over time. Moreover, the incidental occurrence of metastatic carcinoids sometimes complicates the evaluation of experiments and may even obscure the interpretation of the results.

We here report on the generation and detailed characterization of an improved version of the Rip1Tag2 tumor model. By the specific expression of a bicistronic mRNA coding for large T antigen and firefly luciferase in β-cells of Langerhans islets, we have generated a transgenic mouse line (RTL1) that offers the possibility to monitor tumor growth over time by bioluminescence analysis *in vivo* in a quantitative manner. Although RTL1 mice frequently develop micrometastasis in the regional lymph nodes and in the liver, they do not develop overt macrometastasis before they succumb to hypoglycemia. Yet, the micrometastasis can be detected and quantified with high sensitivity by *ex vivo/in vitro* bioluminescence analysis of organ lysates. Comparison of histological analysis and *ex vivo* luciferase measurements has yielded a detection threshold of ∼1 tumor cell in 100 000 target organ cells. Thus, the low background of luminescence from normal tissue, the rapid turnover of the luciferase enzyme and the non-immunogenic characteristics of luciferin make this method ideally suited for longitudinal *in vivo* imaging of tumor progression.

The rat insulin promoter has been used in numerous transgenic mouse models to specifically target transgene expression to pancreatic

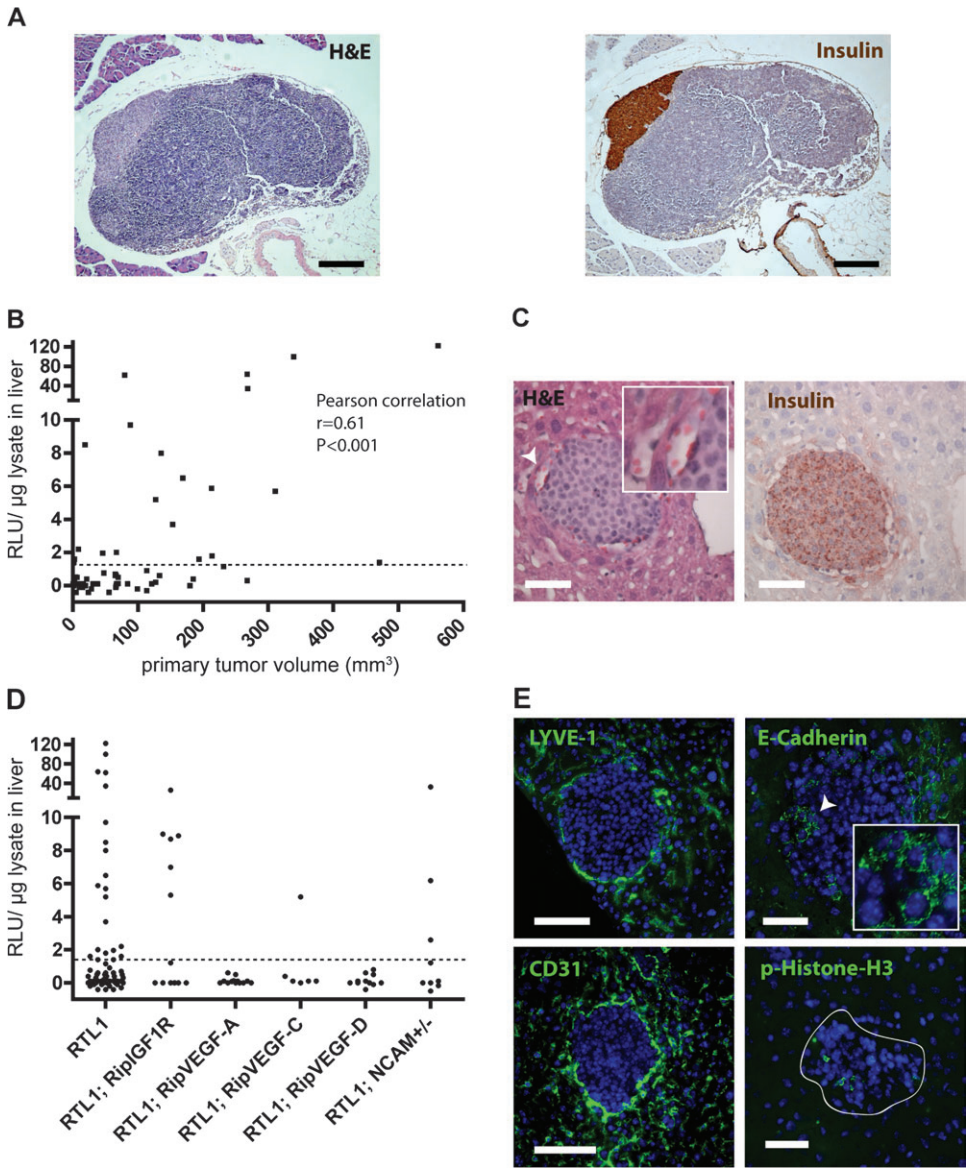

Fig. 5. RTL1 tumors metastasize to the lymph node and liver. (**A**) RTL1 mice show lymph node metastasis in 3/13 mice (23%). Shown are a representative hematoxylin and eosin staining (left panel) and an immunohistochemical insulin staining (right panel) of a histological section of a pancreatic lymph node of an RTL1 mouse. (**B**) Metastatic dissemination of RTL1 tumors to liver correlates with primary tumor size. Normalized luciferase activity in liver homogenates significantly correlates with primary tumor volume and is indicative of liver metastasis. The dashed line indicates the threshold defined as luciferase value 3-fold above background level (obtained with young RTL1 mice livers without primary tumors). (**C**) Histological analysis of liver metastasis in RTL1 mice. Hematoxylin and eosin staining (left panel) and immunohistochemical staining for insulin (right panel) reveal metastatic nodules in livers of RTL1 mice. The arrowhead indicates a blood vessel filled with erythrocytes (inset). (**D**) Composite mice also develop liver metastasis as determined by *ex vivo/in vitro* luciferase analysis as described in panel (B). (**E**): Metastatic nodules in the liver are surrounded by sinusoidal endothelial venules as indicated by immunofluorescence staining for LYVE-1 and CD31 (left panels). Most metastatic cells exhibit low or no E-cadherin expression, yet some cells (re)express this epithelial marker (arrowhead, right top panel, inset). Staining for phospho-Histone-3 indicates cell proliferation within the metastatic nodule in the liver. Scale bars: (A): 200 µm, (D) and (E): 50 µm.

β-cells. However, the onset of transgene expression can vary widely between different founder lines. In RTL1 mice, T antigen mRNA and luciferase protein are expressed in pancreas of newborns, suggesting transgene expression onset before birth. The occurrence of hyperplastic islets at 7 weeks of age also indicates early β-cell transformation, yet the proliferation rate of hyperplastic islets is significantly lower in RTL1 mice as compared with Rip1Tag2 mice. This could be due to lower expression of T antigen in young RTL1 mice and is consistent with the observed slow progression from hyperplastic islets to macroscopic tumors. Indeed, a 5-day pulse of 5-bromodeoxyuridine labeling of cells in S phase of the cell cycle has revealed only ∼20% of BrdU-positive cells within RTL1 tumors (at 14 weeks) compared with a 50% labeling efficiency in Rip1Tag2 mice at 8 weeks of age (data not shown). However, faced by the fact that IGF-II, VEGF-A and other growth parameters are comparably expressed in the tumors of RTL1 and Rip1Tag2 mice, the difference between the proliferative indices remains elusive and warrants further investigation.

The delay of tumor progression in RTL1 mice as compared with Rip1Tag2 mice may also be due to significantly lower levels of $Gr1^{+}/CD11b^{+}$ MDSC in blood, spleen and tumors of RTL1 mice (in FVB/N background) as compared with Rip1Tag2 mice (in C57BL/6 background). Besides repressing immunosurveillance, MDSC and tumor-associated macrophages have been shown to support the angiogenic switch by providing MMP9 for the release of

Table I. Liver metastasis and primary tumor size in RTL1 mice

Genotype	N^a	Primary tumor size		
		<50 mm^3	>50 mm^3 to <150 mm^3	>150 mm^3
		Metastasis frequency		
RTL1	66	4/30 (16.7%)	5/21 (23.8%)	10/15 (66.7%)
RTL1;RipIGF1R	12	1/4 (25%)	3/6 (50%)	2/2 (100%)
RTL1;RipVEGF-A	14	0/11 (0%)	0/3 (0%)	None
RTL1;RipVEGF-C	6	1/4 (25%)	0/2 (0%)	None
RTL1;RipVEGF-D	13	0/10 (0%)	0/1 (0%)	0/2 (0%)
RTL1;NCAM$^{+/-}$	9	0/4 (0%)	2/4 (50%)	1/1 (100%)

Mice are categorized according to primary tumor size and genotype. Percentages represent mice of one category positive for liver metastasis per total mice analyzed in the respective category.
[a]*N*: number of mice analyzed.

matrix-sequestered angiogenic factors, such as VEGF-A (6,34). It is thus tempting to speculate that the reduced myeloid cell infiltration into RTL1 tumors impairs tumor escape from immunosurveillance and efficient tumor angiogenesis.

As frequently observed with malignant human insulinoma and also in Rip1Tag2 mice (29,35,36), RTL1 mice develop liver metastasis. The surrounding of metastatic nodules by LYVE-1$^+$ sinusoidal endothelial vessels and the absence of intrametastatic blood vessels indicate that the metastatic nodules do not (yet) execute an angiogenic program of their own to induce a functional intrametastatic vasculature and thus metastatic outgrowth. However, ~5% of cells are positive for the mitosis marker phospho-Histone-3, demonstrating the proliferation capabilities of the metastatic nodules. The almost complete absence of E-cadherin in metastatic nodules suggests that metastatic cells have undergone epithelial-to-mesenchymal transition, a phenomenon often observed in cancers of epithelial origin (37).

To directly compare the signaling pathways and mechanistic processes required for β-cell tumorigenesis in RTL1 and Rip1Tag2 mice, we have crossed RTL1 mice to a variety of transgenic mice expressing 'tumor modifiers' in β tumor cells and that have been previously crossed to Rip1Tag2 mice. All composite RTL1 transgenic mice analyzed show phenotypes highly comparable with the composite mice described for Rip1Tag2. For example, RTL1;RipIGF1R mice show massively accelerated tumor progression. Also expected, RTL1;RipVEGF-C and RTL1;RipVEGF-D exhibit increased peritumoral lymphangiogenesis, rarely detected in RTL1 single-transgenic mice (data not shown). However, in contrast to the occurrence of lung metastases in 80% of Rip1Tag2;RipVEGF-D mice (23), only one 1 of 14 RTL1;RipVEGF-D mice has developed lung metastasis. Also in contrast to Rip1Tag2 mice, in RTL1 mice, the transgenic expression of VEGF-D does not trigger massive lymphocyte infiltration, an inflammatory stimulus that potentially supports metastatic events (38).

In conclusion, the RTL1 mouse model of pancreatic β-cell carcinogenesis is a valuable tool to monitor primary tumor growth and metastasis formation in a non-invasive manner and in a longitudinal axis. Based on its high reproducibility in multistage tumor progression and the possibility to modulate tumor progression by pharmacological and genetic means, the RTL1 mouse model offers the opportunity to test innovative therapeutic approaches at a preclinical level. Finally, RTL1 transgenic mice can be easily employed to delineate the functional contribution of genes of interest to tumor progression and metastasis by genetic for proof-of-principle experimentation.

Supplementary material

Supplementary Methods, Tables S1 and S2, Figures S1–S3 and Figures 1 and 2 can be found at http://carcin.oxfordjournals.org/

Funding

EU-FP6 BRECOSM LSHC-CT-2004-503224, EU-FP7 TuMIC HEALTH-F2-2008-201662, Oncosuisse, and the NCCR Molecular Oncology of the Swiss National Science Foundation.

Acknowledgements

We thank D.Hanahan for sharing transgenic mouse lines. We are grateful to U.Schmieder and R.Jost for technical support.

References

1. Hanahan,D. *et al*. (2007) The origins of oncomice: a history of the first transgenic mice genetically engineered to develop cancer. *Genes Dev.*, **21**, 2258–2270.
2. Hanahan,D. (1985) Heritable formation of pancreatic beta-cell tumours in transgenic mice expressing recombinant insulin/simian virus 40 oncogenes. *Nature*, **315**, 115–122.
3. Hanahan,D. *et al*. (2000) The hallmarks of cancer. *Cell*, **100**, 57–70.
4. Folkman,J. *et al*. (1989) Induction of angiogenesis during the transition from hyperplasia to neoplasia. *Nature*, **339**, 58–61.
5. Inoue,M. *et al*. (2002) VEGF-A has a critical, nonredundant role in angiogenic switching and pancreatic beta cell carcinogenesis. *Cancer Cell*, **1**, 193–202.
6. Bergers,G. *et al*. (2000) Matrix metalloproteinase-9 triggers the angiogenic switch during carcinogenesis. *Nat. Cell Biol.*, **2**, 737–744.
7. Christofori,G. *et al*. (1994) A second signal supplied by insulin-like growth factor II in oncogene-induced tumorigenesis. *Nature*, **369**, 414–418.
8. Perl,A.K. *et al*. (1998) A causal role for E-cadherin in the transition from adenoma to carcinoma. *Nature*, **392**, 190–193.
9. Zumsteg,A. *et al*. (2009) Corrupt policemen: inflammatory cells promote tumor angiogenesis. *Curr. Opin. Oncol.*, **21**, 60–70.
10. Nozawa,H. *et al*. (2006) Infiltrating neutrophils mediate the initial angiogenic switch in a mouse model of multistage carcinogenesis. *Proc. Natl Acad. Sci. USA*, **103**, 12493–12498.
11. Wild,D. *et al*. (2006) [Lys40(Ahx-DTPA-111In)NH2]exendin-4, a very promising ligand for glucagon-like peptide-1 (GLP-1) receptor targeting. *J. Nucl. Med.*, **47**, 2025–2033.
12. Schomber,T. *et al*. (2009) Differential effects of the vascular endothelial growth factor receptor inhibitor PTK787/ZK222584 on tumor angiogenesis and tumor lymphangiogenesis. *Mol. Cancer Ther.*, **8**, 55–63.
13. Shojaei,F. *et al*. (2008) Role of Bv8 in neutrophil-dependent angiogenesis in a transgenic model of cancer progression. *Proc. Natl Acad. Sci. USA*, **105**, 2640–2645.
14. Wicki,A. *et al*. (2007) [Lys40(Ahx-DTPA-111In)NH2]-exendin-4 is a highly efficient radiotherapeutic for glucagon-like peptide-1 receptor-targeted therapy for insulinoma. *Clin. Cancer Res.*, **13**, 3696–3705.
15. Bergers,G. *et al*. (1999) Effects of angiogenesis inhibitors on multistage carcinogenesis in mice. *Science*, **284**, 808–812.
16. Compagni,A. *et al*. (2000) Fibroblast growth factors are required for efficient tumor angiogenesis. *Cancer Res.*, **60**, 7163–7169.
17. Casanovas,O. *et al*. (2005) Drug resistance by evasion of antiangiogenic targeting of VEGF signaling in late-stage pancreatic islet tumors. *Cancer Cell*, **8**, 299–309.
18. Parangi,S. *et al*. (1996) Antiangiogenic therapy of transgenic mice impairs *de novo* tumor growth. *Proc. Natl Acad. Sci. USA*, **93**, 2002–2007.
19. Dietrich,W.F. *et al*. (1994) Genome-wide search for loss of heterozygosity in transgenic mouse tumors reveals candidate tumor suppressor genes on chromosomes 9 and 16. *Proc. Natl Acad. Sci. USA*, **91**, 9451–9455.
20. Grant,S.G. *et al*. (1991) Early invasiveness characterizes metastatic carcinoid tumors in transgenic mice. *Cancer Res.*, **51**, 4917–4923.
21. Taketo,M. *et al*. (1991) FVB/N: an inbred mouse strain preferable for transgenic analyses. *Proc. Natl Acad. Sci. USA*, **88**, 2065–2069.
22. Gannon,G. *et al*. (2002) Overexpression of vascular endothelial growth factor-A165 enhances tumor angiogenesis but not metastasis during beta-cell carcinogenesis. *Cancer Res.*, **62**, 603–608.
23. Kopfstein,L. *et al*. (2007) Distinct roles of vascular endothelial growth factor-D in lymphangiogenesis and metastasis. *Am. J. Pathol.*, **170**, 1348–1361.
24. Lopez,T. *et al*. (2002) Elevated levels of IGF-1 receptor convey invasive and metastatic capability in a mouse model of pancreatic islet tumorigenesis. *Cancer Cell*, **1**, 339–353.

25. Mandriota,S.J. *et al*. (2001) Vascular endothelial growth factor-C-mediated lymphangiogenesis promotes tumour metastasis. *EMBO J.*, **20**, 672–682.
26. Perl,A.K. *et al*. (1999) Reduced expression of neural cell adhesion molecule induces metastatic dissemination of pancreatic beta tumor cells. *Nat. Med.*, **5**, 286–291.
27. Crnic,I. *et al*. (2004) Loss of neural cell adhesion molecule induces tumor metastasis by up-regulating lymphangiogenesis. *Cancer Res.*, **64**, 8630–8638.
28. Wykoff,C. *et al*. (2000) Hypoxia-inducible expression of tumor-associated carbonic anhydrases. *Cancer Res.*, **60**, 7075–7083.
29. Weber,H.C. *et al*. (1995) Determinants of metastatic rate and survival in patients with Zollinger-Ellison syndrome: a prospective long-term study. *Gastroenterology*, **108**, 1637–1649.
30. Kopfstein,L. *et al*. (2006) Metastasis: cell-autonomous mechanisms versus contributions by the tumor microenvironment. *Cell. Mol. Life Sci.*, **63**, 449–468.
31. Jackson,D.G. *et al*. (2001) LYVE-1, the lymphatic system and tumor lymphangiogenesis. *Trends Immunol.*, **22**, 317–321.
32. Schledzewski,K. *et al*. (2006) Lymphatic endothelium-specific hyaluronan receptor LYVE-1 is expressed by stabilin-1+, F4/80+, CD11b+ macrophages in malignant tumours and wound healing tissue *in vivo* and in bone marrow cultures *in vitro*: implications for the assessment of lymphangiogenesis. *J. Pathol.*, **209**, 67–77.
33. Mouta Carreira,C. *et al*. (2001) LYVE-1 is not restricted to the lymph vessels: expression in normal liver blood sinusoids and down-regulation in human liver cancer and cirrhosis. *Cancer Res.*, **61**, 8079–8084.
34. Coussens,L.M. *et al*. (2000) MMP-9 supplied by bone marrow-derived cells contributes to skin carcinogenesis. *Cell*, **103**, 481–490.
35. Hirshberg,B. *et al*. (2005) Malignant insulinoma: spectrum of unusual clinical features. *Cancer*, **104**, 264–272.
36. Paez-Ribes,M. *et al*. (2009) Antiangiogenic therapy elicits malignant progression of tumors to increased local invasion and distant metastasis. *Cancer Cell*, **15**, 220–231.
37. Thiery,J. *et al*. (2006) Complex networks orchestrate epithelial-mesenchymal transitions. *Nat. Rev. Mol. Cell Biol.*, **7**, 131–142.
38. Denardo,D. *et al*. (2009) CD4(+) T cells regulate pulmonary metastasis of mammary carcinomas by enhancing protumor properties of macrophages. *Cancer Cell*, **16**, 91–102.

Received December 25, 2009; revised April 23, 2010; accepted May 25, 2010